

# Moisture-dependent orthotropic elasticity and strength properties of Chinese fir wood

Jiali Jiang<sup>1,2</sup> · Erik Valentine Bachtiar<sup>2</sup> · Jianxiong Lu<sup>1</sup> · Peter Niemz<sup>2</sup>

Received: 18 May 2016 / Published online: 22 March 2017  
© Springer-Verlag Berlin Heidelberg 2017

**Abstract** Elastic and strength properties are very important material characteristics in mechanical modelling. Due to the anisotropic and hygroscopic nature of wood, a characterization of wood mechanical behavior will require knowledge of its moisture-dependent properties in relation to the three principal axes of anisotropy. The influence of moisture content (MC) on the elastic and strength anisotropy of Chinese fir (*Cunninghamia lanceolata* [Lamb.] Hook) wood was examined in the present study. Selected parameters, including the anisotropic Young's moduli, shear moduli, Poisson's ratios, yield and ultimate stress values in the longitudinal, radial and tangential directions, were determined in compression and tension tests at different moisture conditions. The results indicated that a distinct moisture dependency is exhibited for the elastic and strength behavior of Chinese fir wood. With the exception of some Poisson's ratios, all investigated elastic and strength parameters were shown to decrease with increasing MC, whereby individual moduli and strength values were affected by the MC to different degrees. The two- and three-dimensional representation of the compliance matrix and the two-dimensional visualization of a yield surface give a valuable overview on the moisture-dependent elastic and strength anisotropy of Chinese fir wood.

## 1 Introduction

Chinese fir (*Cunninghamia lanceolata* [Lamb.] Hook) is one of the most important domestic and plantation wood species in China. In the field of wooden structural engineering and wood composite with modeling approaches, the information on elasticity and strength properties has become increasingly important. In the case of wood, considered in a simplified form as a symmetric and orthotropic solid, full characterization of its mechanical behavior requires the determination of elastic and strength parameters related to the three principal axes of anisotropy (longitudinal  $L$ , radial  $R$  and tangential  $T$ ) and three principal planes ( $LR$ ,  $LT$  and  $RT$ ).

Since wood by nature is hygroscopic, its moisture-dependent mechanical properties are particular interesting. Furthermore, the effect of moisture content (MC) on the mechanical properties of wood has been an extensively researched topic over the last decades. While selected moisture-dependent mechanical properties for numerous wood species have been published in Tiemann (1906), McBurney and Drow (1962), Neuhaus (1983), Kretschmann and Green (1996), Hering et al. (2012a) and Ozyhar et al. (2012), in general, only few properties have been tested for a given mechanical parameters-MC combination in most investigations. Therefore, comprehensive datasets comprising the moisture-dependent anisotropic elastic and strength parameters are missing for most Chinese domestic wood species.

While the influence of MC on the mechanical behavior of wood in the  $L$  direction is relatively well known (Gerhards 1982), the behavior in radial and tangential directions remains scarcely studied. So far, only few studies have examined the moisture-dependent elasticity perpendicular to the grain directions (McBurney and Drow 1962; Neuhaus 1983; Hering et al. 2012a; Ozyhar et al.

✉ Jiali Jiang  
jjialiwood@caf.ac.cn

<sup>1</sup> State Key Laboratory of Tree Genetics and Breeding, Research Institute of Wood Industry, Chinese Academy of Forestry, Beijing 100091, People's Republic of China

<sup>2</sup> Institute for Building Materials, ETH Zurich, 8093 Zurich, Switzerland

2012, 2013a). In addition, due to the difficulty in determining the shear moduli in the three principal planes through static testing, comprehensive data sets of the elastic constants in the three principle directions and the three principal planes are still lacking. Since the author's concern is a moisture-dependent orthotropic material description, all of the required compliance parameters at different moisture states for this study were determined by combined static (compression/tension) and ultrasonic testing. Young's moduli and Poisson's ratios were derived from static tests. In contrast to diverse mechanical or inductive measurement devices (Niemz and Caduff 2008), strain information is obtained by means of a non-contact optical surface deformation measurement method based on digital image correlation (DIC) as already used in previous studies (Keunecke et al. 2008; Hering et al. 2012a; Ozyhar et al. 2012, 2013a). To quantify the shear moduli, different measurement techniques are reported in literature. Static tests with a torsion pendulum, the Iosipescu-Test or the Arcan-Test (Dumail et al. 2000; Clauss et al. 2014) were frequently used. In this study, however, an acoustic method (ultrasound velocity measuring) was carried out (Hering et al. 2012a; Ozyhar et al. 2013b).

As regards the moisture-dependent wood strength, the compressive or tensile strength in the  $R$  and  $T$  directions generally remain widely unknown for most wood species. The available data are limited to a few references (Östman 1985; Kretschmann and Green 1996; Ozyhar et al. 2012, 2013a). With regard to the load capacity and failure prediction of wooden structures, it is of great importance to obtain the knowledge of compressive or tensile stress perpendicular to the grain, which represents the weakest timber point (Bodig and Jayne 1982). Furthermore, the ability to withstand failure from fracture when loaded in compression or tension perpendicular to the grain is a crucial topic in wood structural engineering. However, a complete data set covering the strength values in compression or tension as a function of MC in all anatomical directions is limited to a few references (Ozyhar et al. 2012, 2013a).

The main aims of this study are

1. To evaluate the three-dimensional elastic and strength behavior of Chinese fir wood, the parameters evaluated and reported here comprise the anisotropic Young's moduli, Poisson's ratios, shear moduli, ultimate stress values, and yield stress values.
2. To determine the influence of the MC on the elastic and strength properties.
3. To visualize moisture dependence and to verify the assumed symmetry of the compliance matrix and yield surface.

## 2 Materials and methods

### 2.1 Raw material

Chinese fir (*Cunninghamia lanceolata* [Lamb.] Hook) plantation wood was tested. The average raw density, determined at a temperature of 20 °C and a relative humidity (RH) of 65%, is about 323 kg/m<sup>3</sup>. All test specimens for the determination of the physical and mechanical properties were cut from the heartwood part of the same trunk for the investigation. All knots or defects in the wood structure were excluded from testing in advance.

### 2.2 Specimen preparation

A dog-bone shaped specimen, as presented in Fig. 1, was used for both the compression and tension tests. The cross-sectional area in the narrow specimen section was 14 × 14 mm with parallel specimen surfaces and with a length of 11 mm in the load direction. The matching of the specimen coordinate system and the principle orientation of the wooden material in the load area was ensured. A total of 240 specimens were divided into four groups with 20 samples per load axes  $L$ ,  $R$  and  $T$ ; each group was conditioned in climatic chambers at 50, 65, 85 and 95% RH and a temperature of 20 °C.

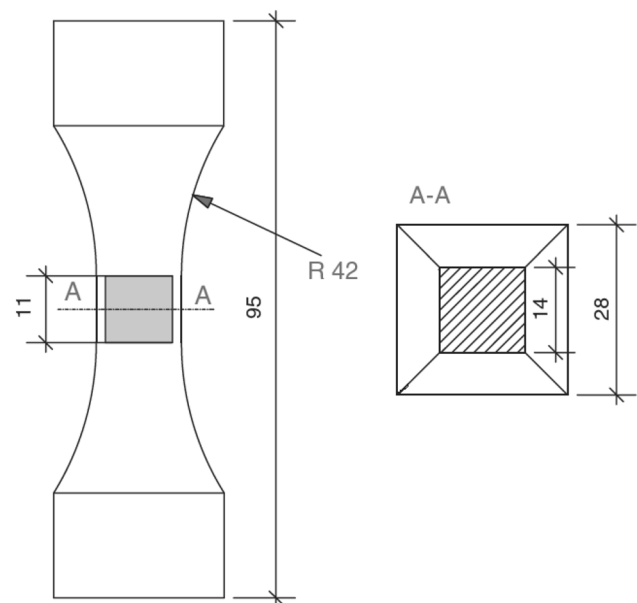


**Fig. 1** Dog-bone shaped specimen used to determine the elastic and strength properties by both compression and tension testing. Figure showing the optically analyzed area is displayed in gray. The dimensions are in (mm)

### 2.3 Speckle pattern

A high-contrast random dot texture (“speckle pattern”) was sprayed on two adjacent sides of the waisted specimen section ( $11 \times 14 \text{ mm}^2$ , Fig. 1). An airbrush gun and finely pigmented acrylic paint was used to obtain very fine speckles and therefore a high-resolution pattern. First, a white ground coat and then black speckles were applied, resulting in a speckle pattern of heterogeneous grey values. These patterns were needed for the evaluation of strains at the specimen surface during compression or tension tests by means of DIC software.

### 2.4 Compression and tension tests: determination of Young’s moduli and Poisson’s ratios

The cuboid profile in the cross-section of the dog-bone shaped specimen allows for the simultaneous measurement of lateral strains in two separate directions and is suitable to determine two Poisson’s ratios on one specimen. The applicability of this specimen to measure the elastic or viscoelastic properties of wood, both in tension as well as in compression, has been recently demonstrated by Hering et al. (2012a) and Ozyhar et al. (2012, 2013c). Choosing this specimen, tensile and compressive properties could be determined using the same specimen type, allowing for a direct comparison of the elastic and strength behavior in tension and compression.

After the specimens reached equilibrium moisture content, compression and tension tests were performed using a Zwick Z100 (Zwick GmbH & Co. KG, Ulm, Germany) universal testing machine equipped with a 100 kN load cell. Data acquisition began when a defined preload was reached. A displacement controlled test was performed with a testing speed of about 1 mm/min. In the compression tests, a flexible joint was used to prevent bending and to compensate for possible non-parallel planes due to small dimensional changes as a result of climatisation. As for tension tests, the central load transmission for both configurations was achieved with conical clamp jaws.

To determine the Young’s moduli and Poisson ratio, both the compression and tension tests were performed only at small strains in the linear elastic range. To measure the strength properties, the specimens were loaded until yield or failure with a constant loading rate so that specimen failure was reached in  $90 \pm 30 \text{ s}$ , whereby the loading rate was adjusted to the orthotropic directions and the loading modes.

#### 2.4.1 Strain measurement

For the strain measurement, an optical video image correlation system (VIC 2D, Correlated Solutions Inc., Columbia,

SC, USA) was applied, allowing an evaluation of the strain distribution over the complete specimen surface. To this purpose, an optimized correlation algorithm was available, which provided full-field displacement and strain data for mechanical testing on planar specimens. The displacement data from two adjacent sides of the specimen during both the compression and tension measurements were determined by a pair of charge coupled device (CCD) digital cameras, each with a maximum resolution of  $2048 \times 2048$  pixels. The in-plane movement was determined for the selected measurement area of interest with a size of about  $11 \times 11 \text{ mm}^2$  (Fig. 1) by calculating the average strain in the load direction and across this direction.

#### 2.4.2 Calculation of Young’s moduli

The Young’s moduli  $E$  were obtained from the ratio of the stress  $\sigma$  to the corresponding strain  $\varepsilon$  measured in the linear elastic range

$$E_i = \frac{\Delta\sigma_i}{\Delta\varepsilon_i} = \frac{\sigma_{i,2} - \sigma_{i,1}}{\varepsilon_{i,2} - \varepsilon_{i,1}} \quad i \in L, R, T \quad (1)$$

The specific stress-boundaries,  $\sigma_{i,1}$  and  $\sigma_{i,2}$ , were set at 30 and 70% of the actual force at 50% elastic limit. The orientation dependent maximum forces were determined in the preliminary tests for the three main directions.

#### 2.4.3 Calculation of Poisson’s ratios

The Poisson’s ratio  $\nu$ , defined as the strain ratio of the passive (lateral) strain component  $\varepsilon_i$  and the active (axial) strain component in the load direction  $\varepsilon_j$ , was calculated by Eq. 2 and determined in the linear elastic range from the linear regression of the passive-active strain diagram.

$$\nu_{ij} = -\frac{\varepsilon_i}{\varepsilon_j} \quad i, j \in L, R, T \text{ and } i \neq j \quad (2)$$

#### 2.4.4 Calculation of ultimate stress and yield stress

Two different strength criteria, the ultimate stress  $\sigma_{US}$  and the yield stress  $\sigma_y$ , were used to characterize the compression and tension strength properties of wood in all orthotropic directions (Ozyhar et al. 2012, 2013a) using the following relationship

$$\sigma_{us} = \frac{P_{\max}}{A} \quad (3)$$

where  $\sigma_{us}$  was calculated from the maximum load  $P_{\max}$  at the point of failure and the cross-section area  $A$  (e.g.,  $14 \times 14 \text{ mm}^2$ , Fig. 1) of the unloaded specimen.  $\sigma_y$ , representing the stress at the specific yield point, was obtained from the measured stress–strain diagram based on the “offset yield method” at 0.2% plastic strain (Fig. 2).

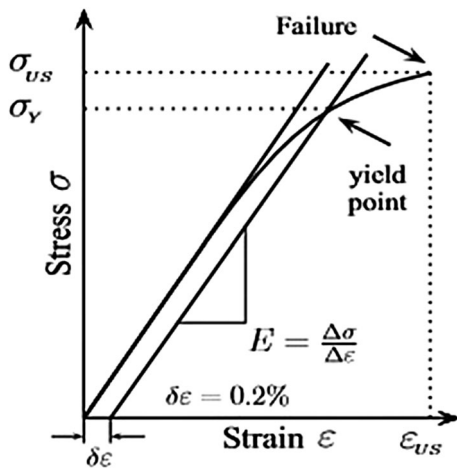


**Fig. 2** Determination of the ultimate stress  $\sigma_{US}$  and the yield stress  $\sigma_y$  from the stress–strain diagram

2.4.5 Ultrasound testing: determination of shear moduli

Clear cubic specimens with orthotropic material directions parallel to the sample edges were prepared and classified into three groups with 80 specimens each thickness set, with edge length of 10, 13 and 16 mm, respectively. For each thickness set, cubes were successively cut from a stick perfectly parallel to the longitudinal direction. This precaution allows the same annual growth rings to be obtained for testing, and yields a series of matched samples with very similar properties. In order to achieve a precise surface area for ultrasonic testing, cubes were finished with fine sandpaper. Prior to testing, each dimension set with 80 specimens was divided into four groups and moisture-conditioned in climatic chambers at a temperature of 20 °C and different relative humidity of 50, 65, 85 and 95% until equilibrium moisture content was reached. A total of 240 specimens with 20 specimens for each dimension and moisture condition were available for testing.

Ultrasound testing was performed with an Epoch XT ultrasonic flaw detector (Olympus NDT Inc., USA). Two Staveley S-0104 transducers for transversal waves (1 MHz) with a diameter of 12.7 mm were used. A constant contact pressure was guaranteed by the clamping apparatus. Sound velocities were expressed by the general form  $V_{ij}$ , where  $i$  is the direction of wave propagation and  $j$  is the direction of oscillation. As a result, six sound velocities of transverse wave propagating/oscillating in the  $LR$ ,  $RL$ ,  $LT$ ,  $TL$ ,  $RT$  and  $TR$  planes were measured. As an approximation, orthorhombic symmetry can be assumed for the cubic specimens.

The resulting sound velocities were determined by a simple linear regression from the measured time required for the ultrasound pulse to propagate through the samples

with three different thicknesses (Fig. 3), in order to eliminate the sound velocity error introduced by the flaw detector.

On the basis of the sound velocity ( $V_{ij}$ ) of the ultrasonic waves and of the raw density ( $\rho$ ) of the specimens, the shear moduli ( $G_{ij}$ ) were calculated according to Eq. (4):

$$G_{ij} = V_{ij}^2 \cdot \rho \quad i, j \in R, L, T \quad \text{and} \quad i \neq j \quad (4)$$

The shear moduli were calculated from the averaged values of the transverse wave velocities  $V_{ij}$  and  $V_{ji}$ . Therefore, three shear moduli were calculated from the relationship listed in Table 1.

2.5 Calculation of equilibrium moisture content

For the calculation of the equilibrium moisture content  $\omega$  (Eq. 5), the mass of the samples was determined at 20 °C and 50, 65, 85, 95% RH ( $m_\omega$ ) and oven-dry ( $m_0$ ):

$$\omega = (m_\omega - m_0) / m_0 \times 100\% \quad (5)$$

The corresponding equilibrium moisture contents were 10.3, 12.2, 14.6 and 16.7%, respectively. For the multiple

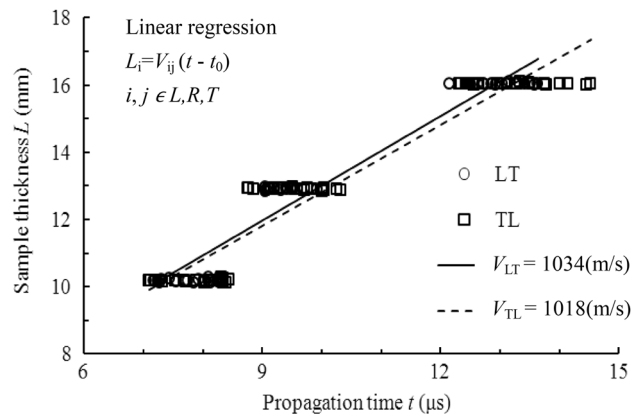


**Fig. 3** Ultrasonic wave propagation velocity analyzed by means of linear regression with multiple sample thicknesses. (Scheme with both measurement options in  $LT$  plane for moisture content of  $\omega = 12.2\%$ )

**Table 1** Equations used to calculate the shear moduli from the transverse wave velocities

Type of wave	Equations
$V_{LR}$ and $V_{RL}$	$G_{LR/RL} = (\rho V_{LR}^2 + \rho V_{RL}^2) / 2$
$V_{LT}$ and $V_{TL}$	$G_{LT/TL} = (\rho V_{LT}^2 + \rho V_{TL}^2) / 2$
$V_{RT}$ and $V_{TR}$	$G_{RT/TR} = (\rho V_{RT}^2 + \rho V_{TR}^2) / 2$

comparisons of orthotropic Young’s moduli, Poisson’s ratio and strength properties at different MC levels, Duncan’s multiple range test for variable was applied with PASW Statistics 18.0 software.

### 3 Results and discussion

#### 3.1 Moisture-dependent elastic anisotropy

##### 3.1.1 Young’s moduli

Table 2 provides an overview of the determined moisture-dependent compressive ( $E^{Co}$ ) and tensile ( $E^{Te}$ ) Young’s moduli of Chinese fir in three directions. The results clearly indicate a general increase in MC significantly lowered the Young’s moduli in all orthotropic directions for both compressive and tensile modes according to Duncan’s multiple range test. The graphical illustration of the measured moduli reveals a nearly linear relationship with the MC (Fig. 4). The individual moduli  $E_L$ ,  $E_R$  and  $E_T$  are affected by the MC to a different degree. With a decrease of 24.8 and 24.7% for  $E_L^{Co}$  and  $E_L^{Te}$  respectively, 34.1 and 37.5% for  $E_R^{Co}$  and  $E_R^{Te}$  respectively, 45.5 and 40.0% for  $E_T^{Co}$  and  $E_T^{Te}$  respectively over the measured MC range, the decline in the  $R$  and  $T$  directions is more pronounced than that in the  $L$  direction. A similar trend was reported by Hering et al. (2012a) and Ozyhar et al. (2012), and they showed that, in general, the  $E_L$  for European beech (*Fagus sylvatica* L.) wood is less sensitive to MC changes than the moduli in the directions perpendicular to the grain. While for Douglas fir (*Pseudotsuga menziesii*), the perpendicular to the grain moduli have been shown to change with MC 8–10 times the rate than for the  $E_L$  (McBurney and Drow 1962). Though the values are clearly higher than the relationship published in this study, the results presented here proved that  $E_R$  and  $E_T$  are affected by the MC to a higher degree than the  $E_L$ .

Comparison of the moisture-dependent  $E^{Co}$  and  $E^{Te}$  values within the individual orthotropic directions is also shown in Fig. 4. The results reveal that the  $E^{Te}$  values in these directions are higher than the corresponding  $E^{Co}$  values, and the averaged difference between the  $E^{Co}$  and  $E^{Te}$  in  $L$ ,  $R$  and  $T$  directions is about 15.5, 6.6 and 10.9%, respectively. Furthermore, based on the above discussion, with regard to the sensitivity of Young’s moduli in response to MC changes, it is shown that the  $E^{Te}$  and  $E^{Co}$  are similar in all three anatomy directions over the measured MC range.

In order to clarify the elastic anisotropy of Chinese fir wood, Table 2 summarizes the Young’s moduli ratios obtained at the four specific MC using the compression and tension methods. According to Bodig and Jayne (1982), the relationships between the longitudinal and transverse elasticity moduli vary greatly among species, but overall, the

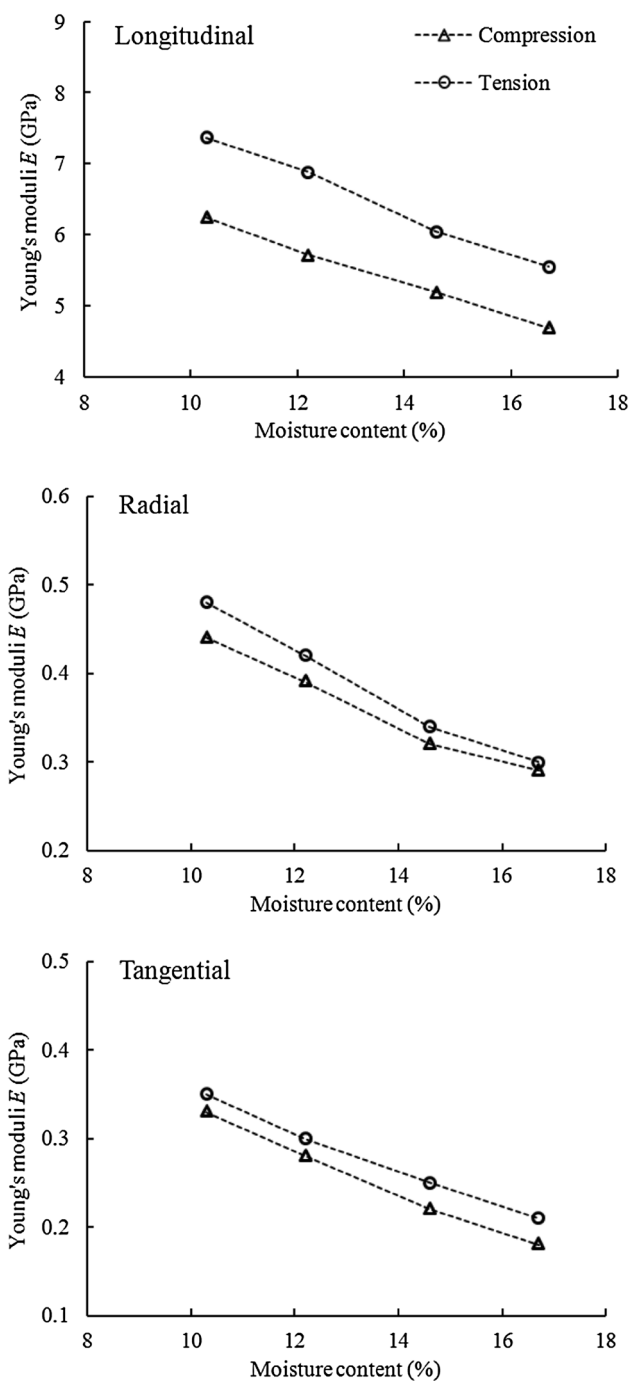


Fig. 4 Moisture-dependent compressive and tensile Young’s moduli of Chinese fir wood in three directions

magnitudes of Young’s moduli ratios are approximately  $E_L : E_R : E_T \approx 20 : 1.6 : 1.0$ . It is noted that in this study the  $E_L/E_T$  ratios at lower MC (10.3 and 12.2%) are similar to values suggested by Bodig and Jayne (1982), but it showed large  $E_L/E_T$  ratios at higher MC (14.6 and 16.7%) for both types of tests. This result suggests that the orthotropy of Chinese fir wood in the present study was similar to that

**Table 2** Moisture-dependent Young’s moduli of Chinese fir wood determined by compression and tension

$\bar{\omega}$ (%)	$n=20$	Compression						Tension					
		Young’s moduli (GPa)			Anisotropy			Young’s moduli (GPa)			Anisotropy		
		$E_L^{Co}$	$E_R^{Co}$	$E_T^{Co}$	$E_L^{Co}/E_T^{Co}$	$E_L^{Co}/E_R^{Co}$	$E_R^{Co}/E_T^{Co}$	$E_L^{Te}$	$E_R^{Te}$	$E_T^{Te}$	$E_L^{Te}/E_T^{Te}$	$E_L^{Te}/E_R^{Te}$	$E_R^{Te}/E_T^{Te}$
10.3	$\bar{x}$	6.24A	0.44A	0.33A	18.9	14.2	1.3	7.37A	0.48A	0.35A	21.1	15.4	1.3
	CoV (%)	6.7	15.6	17.5				9.8	12.5	8.1			
12.2	$\bar{x}$	5.71B	0.39B	0.28B	20.4	14.6	1.4	6.88B	0.42B	0.30B	22.9	16.4	1.4
	CoV (%)	12.7	15.1	15.1				6.5	11.6	6.0			
14.6	$\bar{x}$	5.19C	0.32C	0.22C	23.6	16.2	1.5	6.04C	0.34C	0.25C	24.2	17.8	1.3
	CoV (%)	11.9	15.3	18.5				9.5	7.2	4.6			
16.7	$\bar{x}$	4.69D	0.29C	0.18D	26.1	16.2	1.6	5.55D	0.30D	0.21D	26.4	18.5	1.4
	CoV (%)	12.3	15.1	16.8				7.2	6.6	4.5			

$\bar{\omega}$ , average wood moisture content;  $\bar{x}$ , mean value;  $n$ , number of specimens; CoV, coefficient of variation. The same letter in the same column indicates that there is no statistical difference in Young’s moduli among MC level; different letter indicates significant differences at  $P < 0.05$

expected by Bodig and Jayne (1982), who reported that an  $E_L/E_T$  ratio near 24:1 would make the wood the most highly orthotropic material known to man. Tracheids orientation in the longitudinal direction gives the higher longitudinal stiffness, and in the case of radial and tangential stiffness, the lower the density, the lower these values will be (Keunecke et al. 2007; Gonçalves et al. 2011). Consequently, lower wood density species such as Chinese fir tend to produce smaller radial and tangential stiffness and, therefore, larger differences between Young’s moduli in longitudinal and transverse directions could be observed. In the case of  $E_R/E_T$ , the current results are also similar to the values suggested by Bodig and Jayne (1982), and it exhibits slightly increasing trend with the increase of MC in the compression tests, while it remains unchanged with MC in the tension tests. A similar finding was published in Ozyhar et al. (2012, 2013b), where no evidence of the influence of the MC on the elastic anisotropy for European beech wood measured both by tension and ultrasound methods could be

found. In general, the values of the Young’s moduli ratios obtained in the compression and tension tests were found to be similar.

3.1.2 Poisson’s ratios

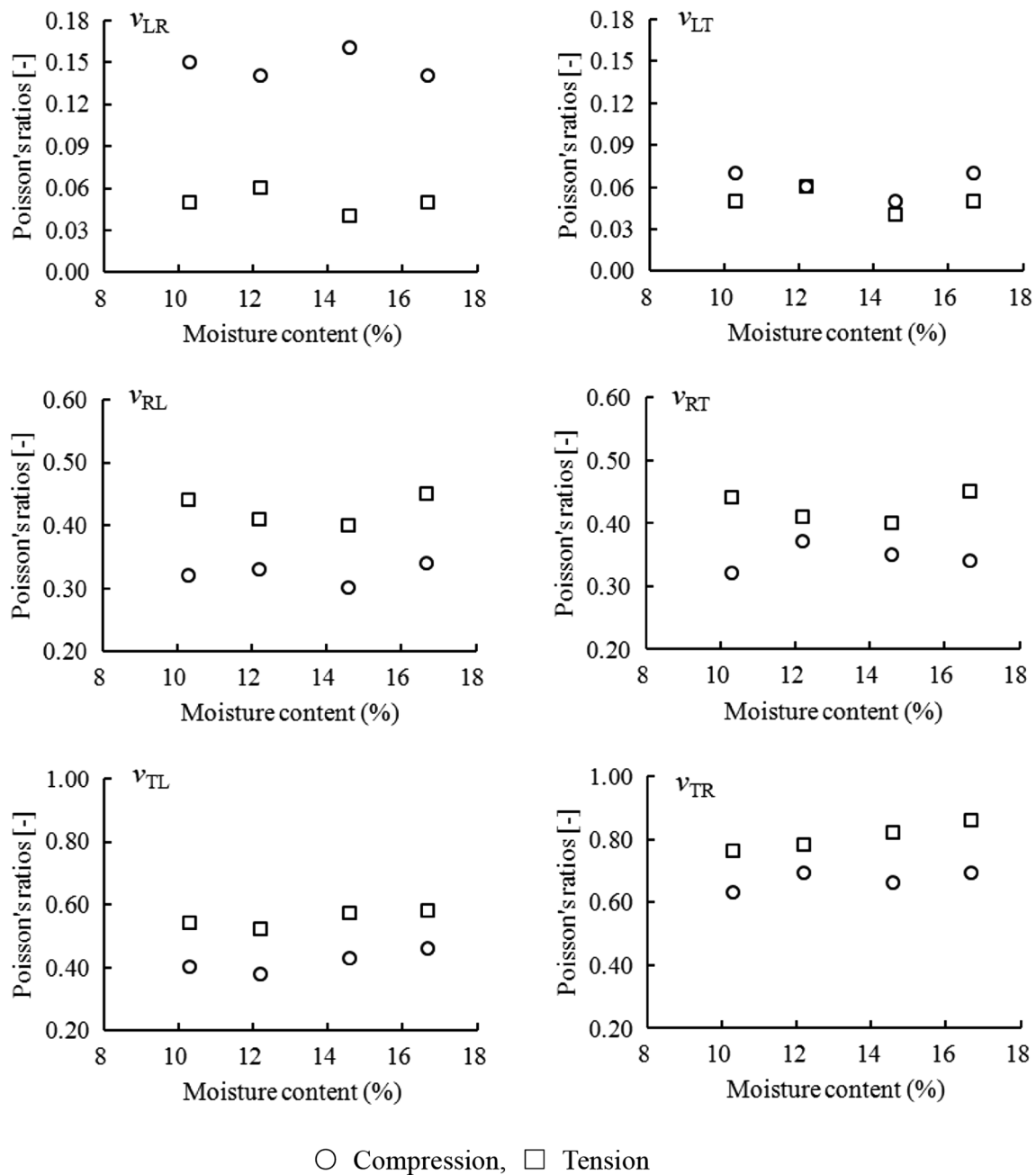
The moisture-dependent Poisson’s ratios determined by compression and tension modes are listed in Table 3. It shows the highest values in the RT plane if the lateral extension is oriented in the T direction ( $v_{TR}$ ), and the lowest values if the lateral extension is oriented in the L direction ( $v_{LR}$  or  $v_{LT}$ ). Previous studies (Keunecke et al. 2008; Jeong et al. 2010; Ozyhar et al. 2012, 2013a; Mizutani and Ando 2015) have reported wide variation in the Poisson’s ratio of wood due to a high coefficient of variation, and this study reached a similar conclusion.

Figure 5 shows the influence of MC on the Poisson’s ratios. A slightly increasing tendency with MC is observed for  $v_{TL}$  and  $v_{TR}$  in both compression and tension tests, while

**Table 3** Moisture-dependent compressive and tensile Poisson’s ratios of Chinese fir wood

$\bar{\omega}$ (%)	$n=20$	Compression						Tension					
		$v_{LR}$	$v_{LT}$	$v_{RL}$	$v_{RT}$	$v_{TL}$	$v_{TR}$	$v_{LR}$	$v_{LT}$	$v_{RL}$	$v_{RT}$	$v_{TL}$	$v_{TR}$
10.3	$\bar{x}$	0.15A	0.10AB	0.32A	0.26A	0.40A	0.63A	0.05A	0.07A	0.44A	0.32A	0.54A	0.76A
	CoV (%)	19.3	22.8	26.7	23.1	16.9	12.4	24.3	15.3	21.5	18.0	19.7	13.8
12.2	$\bar{x}$	0.14A	0.11AB	0.33A	0.34B	0.38A	0.69A	0.06A	0.06AB	0.41A	0.37B	0.52A	0.78AB
	CoV (%)	18.0	24.0	19.4	16.5	24.4	12.9	17.1	25.2	16.7	17.6	11.6	11.2
14.6	$\bar{x}$	0.16A	0.09B	0.30A	0.31BC	0.43AB	0.66A	0.04A	0.05B	0.40A	0.35AB	0.57A	0.82BC
	CoV (%)	18.9	31.7	19.6	22.4	25.9	15.5	27.4	25.9	19.0	13.5	17.0	14.5
16.7	$\bar{x}$	0.14A	0.12A	0.34A	0.27AC	0.46B	0.69A	0.05A	0.07A	0.45A	0.34AB	0.58A	0.86C
	CoV (%)	25.5	32.8	23.1	9.7	28.8	14.5	24.0	26.8	18.9	17.4	19.7	11.2

$\bar{\omega}$ , average wood moisture content;  $\bar{x}$ , mean value;  $n$ , number of specimens; CoV, coefficient of variation. The same letter in the same column indicates that there is no statistical difference in Poisson’s ratio among MC level; different letter indicates significant differences at  $P < 0.05$



**Fig. 5** The moisture-dependent Poisson’s ratios of Chinese fir wood determined in compression and tension. (Circle) Compression, (square) tension

other Poisson’s ratios appear to be rather insensitive to MC. This is similar to the findings published in Ozyhar et al. (2012), where the  $v_{TL}$ ,  $v_{TR}$  and  $v_{RT}$  were shown to increase with increasing MC, meanwhile, no significant influence of MC on the other Poisson’s ratios could be found. However, these results are contrary to the moisture-dependent Poisson’s ratios reported by some researchers (Kretschmann and Green 1996; Hering et al. 2012a; Mizutani and Ando 2015), who found a decreasing tendency with increasing

MC (below the fiber saturation point). Furthermore, according to McBurney and Drow (1962), some of the Poisson’s ratios of Douglas fir were found to increase, where others decrease with increasing MC. Overall, different wood species, varying specimen shape and unequal loading conditions may explain the wide variation of Poisson’s ratios with MC in the literature (Ozyhar et al. 2013a; Mizutani and Ando 2015). Duncan’s multiple range test also showed that MC had a complex effect on Poisson’s

ratio, and it was hard to establish a direct influence of MC on Poisson’s ratio.

From Fig. 5, different Poisson’s ratio values in compression and tension indicate that the loading direction appears to have a greater influence on the values than the MC. Inequalities between the compression and tension values are most pronounced for the  $\nu_{LR}$ , and to a less extent for the  $\nu_{LT}$ , whereby the Poisson’s ratios ( $\nu_{RL}$ ,  $\nu_{RT}$ ,  $\nu_{TL}$  and  $\nu_{TR}$ ) in compression are lower than the corresponding values in tension. This is different from the compression-tension relationship of wood’s Poisson’s ratios reported by Ozyhar et al. (2013a), who found the Poisson’s ratios of European beech wood in compression are generally higher than that in tension. It is suggested that a complex cellular material with hierarchical structure like wood exhibits different elastic responses in compression and tension, which could lead to a different Poisson’s effect.

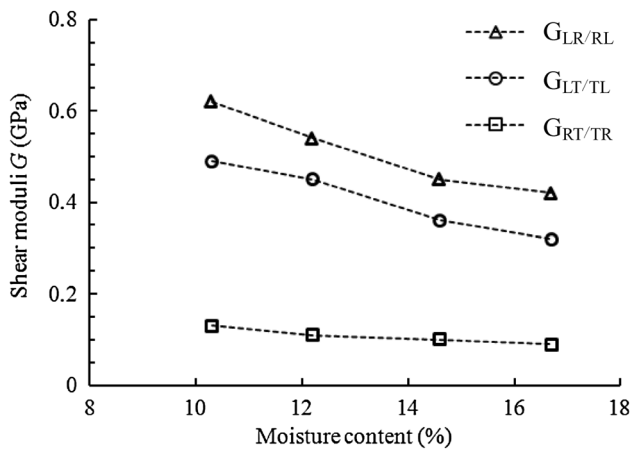


**Fig. 6** Moisture-dependent shear moduli of Chinese fir wood determined by ultrasonic method

### 3.1.3 Shear moduli

The approach to determine the shear moduli on the basis of a linear regression is exemplarily shown in Fig. 3 for measurement data in the *LT* plane. The presumed similarity in the corresponding measurement directions *LT/TL*, *LR/RL*, *RT/TR* can obviously be confirmed by the comparison of the resulting linear functions.

The moisture-dependent shear moduli are summarized in Table 4. With the highest moduli measured at  $\omega = 10.3\%$  and the lowest at  $\omega = 16.7\%$ , shear moduli decrease with increasing MC. Similar to the Young’s moduli (Fig. 4), the shear moduli exhibit a nearly linear relationship with the MC (Fig. 6). With a decrease of 32.3% for  $G_{LR/RL}$ , 34.7% for  $G_{LT/TL}$  and 30.8% for  $G_{RT/TR}$ , shear moduli are affected by the MC to a similar degree. Apparently, a ratio of approximately 5(LR) : 4(LT) : 1(RT) between the material planes is valid for the shear moduli.

### 3.1.4 Visualization of the moisture-dependent elastic anisotropy

To characterize the elastic behavior of wood, twelve independent elastic engineering parameters, namely three Young’s moduli ( $E_L$ ,  $E_R$ ,  $E_T$ ), three shear moduli ( $G_{LR/RL}$ ,  $G_{LT/TL}$ ,  $G_{RT/TR}$ ) and six Poisson’s ratios ( $\nu_{LR}$ ,  $\nu_{RL}$ ,  $\nu_{LT}$ ,  $\nu_{TL}$ ,  $\nu_{RT}$ ,  $\nu_{TR}$ ) are usually represented as components of a  $6 \times 6$  compliance matrix *S* (Bodig and Jayne 1982). Using the data from Tables 2, 3 and 4, the moisture-dependent elastic anisotropy for Chinese fir wood determined by compression and tension can be visualized by a two-dimensional representation of the compliance matrix, respectively (see Fig. 7a, b). These illustrations were generated assuming the discussed material symmetry by averaging the non-diagonal compliance elements. Displayed by the polar diagrams for the three planes of anisotropy, the load direction-dependent compliance provides a valuable overview of the elastic anisotropy of Chinese fir wood. An increase

**Table 4** Moisture-dependent shear moduli of Chinese fir wood determined by ultrasonic method

$\omega$ (%)	$n = 20$	Shear moduli (GPa)			$G_{LR/RL}/G_{LT/TL}$	$G_{LR/RL}/G_{RT/TR}$	$G_{LT/TL}/G_{RT/TR}$
		$G_{LR/RL}$	$G_{LT/TL}$	$G_{RT/TR}$			
10.3	$\bar{x}$	0.62	0.49	0.13	1.3	4.8	3.8
	$R^2$	0.89	0.94	0.96			
12.2	$\bar{x}$	0.54	0.45	0.11	1.2	4.9	4.1
	$R^2$	0.93	0.88	0.92			
14.6	$\bar{x}$	0.45	0.36	0.10	1.3	4.5	3.6
	$R^2$	0.94	0.96	0.92			
16.7	$\bar{x}$	0.42	0.32	0.09	1.3	4.7	3.6
	$R^2$	0.87	0.91	0.88			

$\bar{\omega}$ , average wood moisture content;  $\bar{x}$ , linear regression value;  $R^2$ , coefficient of correlation



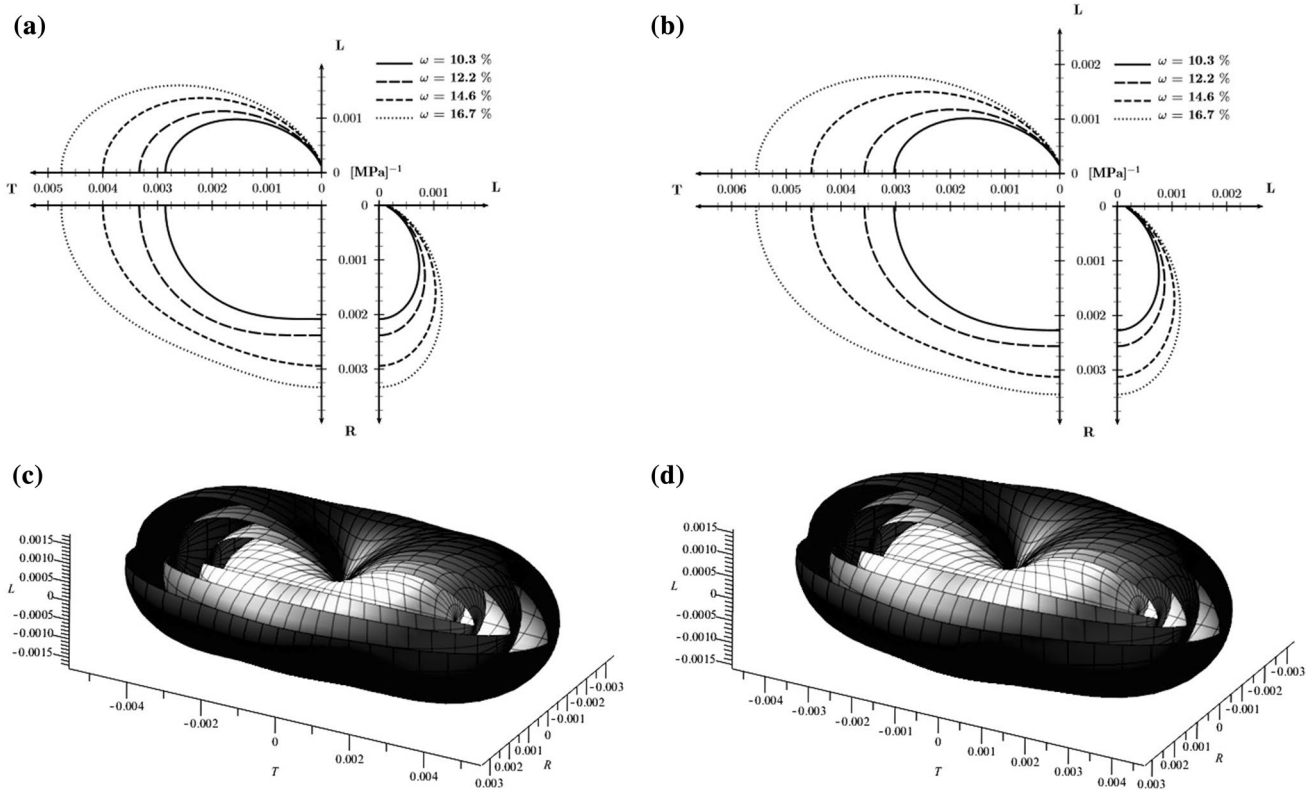


**Fig. 7** Load-directional dependence of Chinese fir wood compliance under compression (**a** and **c**) and tension (**b** and **d**) at different moisture contents. **a, b** via polar diagrams for the principal planes of

anisotropy, **c, d** by the three-dimensional representation (increasing moisture content from *light to dark*)

in compliance with increasing MC can be observed in all planes. The connection between the absolute compliance value and the moisture sensitivity is clearly visible. Furthermore, this illustration gives an impression of an off-axis deformation. Moreover, it becomes even clearer when visualized by the so-called “deformation bodies” displayed in Fig. 7c, d. In this manner, the influence of the MC on the overall deformation capability of Chinese fir wood under compression and tension can be summarized effectively. Presented earlier by Keunecke et al. (2008), Hering et al. (2012a), Ozyhar et al. (2012) and Clauss et al. (2014), the three-dimensional representation of the compliance matrix is suitable to describe the degree of the material deformation dependent on the load direction.

### 3.2 Moisture-dependent strength anisotropy

Table 5 summarizes the moisture-dependent strength behavior determined by compression and tension for Chinese fir wood. Similar to the Young’s and shear moduli (Tables 2, 4), in general, all the ultimate compression stress  $\sigma_{UCS}$  and ultimate tensile stress  $\sigma_{UTS}$  values were significantly lowered by the increasing MC according to Duncan’s multiple range test. Since the tensile specimen

in the  $L$  direction was too stiff for a sufficient ultimate tension strength calculation, the  $L - \sigma_{UTS}$  was not gaugeable in this study. The results showed that an increase in MC over the measured MC range will lead to about 19.0, 33.7 and 35.9% decrease in strength of  $L - \sigma_{UCS}$ ,  $R - \sigma_{UTS}$  and  $T - \sigma_{UTS}$ , respectively. The significantly rising ultimate tensile strain  $\epsilon_{UTS}$  values in both  $R$  and  $T$  directions further clarified that wood becomes more ductile with increasing MC.

While the ultimate stress in tension  $\sigma_{UTS}$ , is the most common tensile strength criterion used in wood science, it may not always be the most appropriate choice to describe the overall strength behavior of wood. Since the compression behavior of wood in the  $R$  and  $T$  directions is characterized by the absence of clear failure and no ultimate stress value exists (Bodig and Jayne 1982), a direct comparison of the compressive and tensile strength behavior using the ultimate stress criterion is not possible. Therefore, compressive yield stress  $\sigma_Y^{Co}$  and tensile yield stress  $\sigma_Y^{Te}$ , often referred to as the strength in engineering, are introduced to enable a comparison of the compressive and tensile strength behavior (Table 5). Analogue moisture-dependent yield stress values for European beech wood measured under compression or/

**Table 5** Moisture-dependent strength properties of Chinese fir wood by compression and tension

$\bar{\omega}$ (%)	$n=15$	Compression						Tension								
		L			R			L			R			T		
		$\sigma_{UCS}$ (N/mm <sup>2</sup> )	$\epsilon_{UCS}$ (%)	$\sigma_Y^{Co}$ (N/mm <sup>2</sup> )	$\sigma_Y^{Co}$ (N/mm <sup>2</sup> )	$\sigma_{UTS}^{Co}$ (N/mm <sup>2</sup> )	$\sigma_Y^{Co}$ (N/mm <sup>2</sup> )	$\sigma_{UTS}$ (N/mm <sup>2</sup> )	$\sigma_Y^{Te}$ (N/mm <sup>2</sup> )	$\sigma_{UTS}$ (N/mm <sup>2</sup> )	$\epsilon_{UTS}$ (%)	$\sigma_{UTS}$ (N/mm <sup>2</sup> )	$\sigma_Y^{Te}$ (N/mm <sup>2</sup> )	$\epsilon_{UTS}$ (%)		
10.3	$\bar{x}$	28.50A	0.93A	3.24A	3.24A	2.64A	2.64A	—	3.68A	3.28A	0.84A	3.23A	2.87A	0.94A		
	CoV(%)	8.1	22.1	5.2	5.2	18.7	18.7	—	13.3	15.8	14.1	10.7	12.3	10.4		
12.2	$\bar{x}$	26.22B	0.81AB	2.96B	2.96B	2.30AB	2.30AB	75.1*	3.44A	2.99AB	0.92A	2.81AB	2.58A	1.07AB		
	CoV(%)	2.9	18.6	5.8	5.8	9.9	9.9	—	12.5	13.6	8.4	8.4	9.7	7.1		
14.6	$\bar{x}$	24.70BC	0.68BC	2.44C	2.44C	2.02AB	2.02AB	—	2.98B	2.54BC	1.05A	2.38BC	2.09B	1.20BC		
	CoV(%)	5.8	9.8	10.7	10.7	2.3	2.3	—	9.7	12.0	12.4	11.9	10.5	12.6		
16.7	$\bar{x}$	23.08C	0.53C	2.15D	2.15D	1.87B	1.87B	—	2.44C	2.18C	1.20A	2.07C	1.80B	1.44C		
	CoV(%)	8.4	13.1	10.6	10.6	12.1	12.1	—	8.0	7.9	15.3	13.2	12.6	19.4		

$\bar{\omega}$ , average wood moisture content;  $\bar{x}$ , mean value; CoV, coefficient of variation;  $\sigma_{UCS}$ , ultimate compressive stress;  $\sigma_{UTS}$ , ultimate tensile stress;  $\sigma_Y^{Co}$ , compressive yield stress;  $\sigma_Y^{Te}$ , tensile yield stress;  $\epsilon_{UCS}$ , strain at  $\sigma_{UCS}$ ;  $\epsilon_{UTS}$ , strain at  $\sigma_{UTS}$ . The same letter in the same column indicates that there is no statistical difference in item of strength properties among MC level; different letter indicates significant differences at  $P < 0.05$ .

\*Bao and Jiang (1998)

and tension have recently been published by Hering et al. (2012b) and Ozyhar et al. (2012, 2013a).

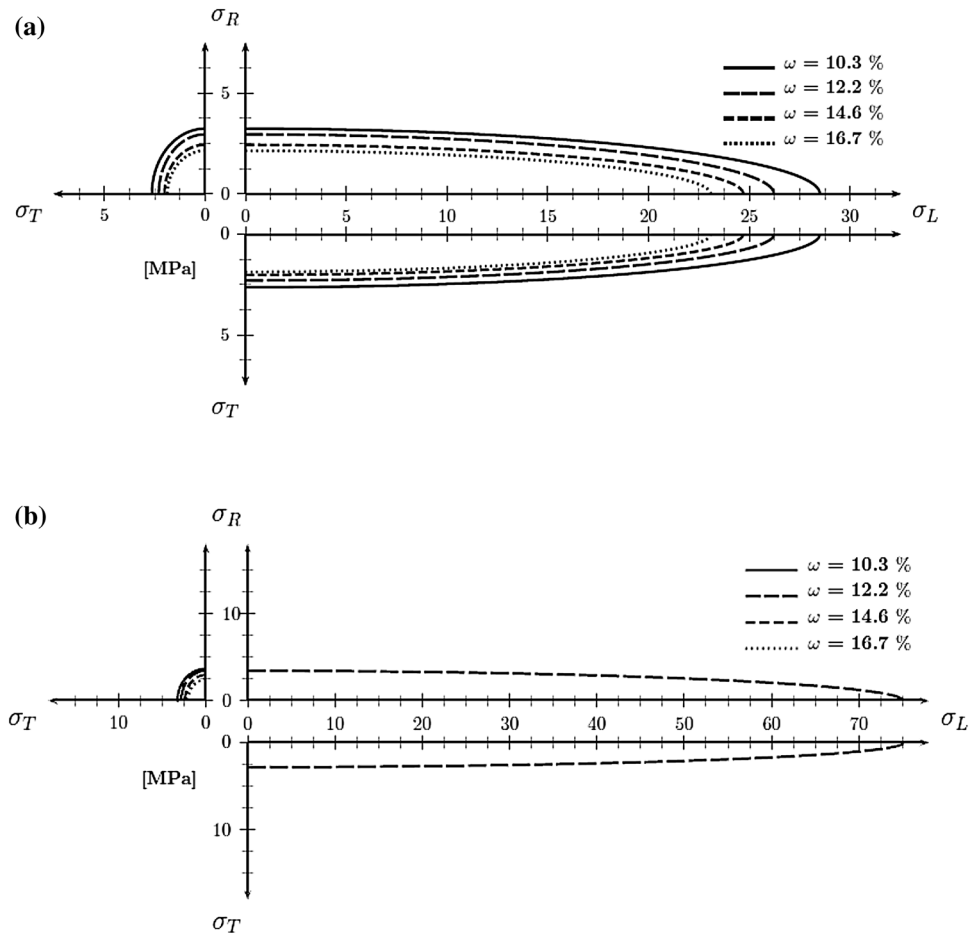
Applying the yield condition given in Resch and Kaliske (2010) and Saft and Kaliske (2011), the compressive and tensile strength behavior of Chinese fir can be visualized for all principal planes of anisotropy (Fig. 8). Using the  $\sigma_Y^{Co}$  and  $\sigma_Y^{Te}$  values (Table 5), the yield surfaces in compression and tension were determined for measured MC levels, respectively. Since the yield stress represents the point where the material begins to plastically deform, the surface provides valuable information about the position of the transition zone between the elastic and plastic region in the stress–strain diagram. In the presented yield surfaces, as shown in Fig. 8, the stress state displayed below the lines forming the surface represents the elastic and the stress state above the plastic regions of the mechanical behavior. Calculating the average  $\sigma_Y^{Co}$  and  $\sigma_Y^{Te}$  values for the different MCs, respectively, the uniaxial anisotropic compressive and tensile strength are described by the following ratio,  $L:R: T \approx 11.7: 1.2: 1$  for compression and  $\approx 29.1: 1.2: 1$  for tension.

### 4 Conclusion

With static and ultrasound test methods, the moisture-dependent orthotropic elastic and strength properties of Chinese fir wood were quantified at different MCs in both compression and tension. This is exemplified by the two- and three-dimensional visualization of the compliance matrix and the two-dimensional representation of its yield surface. The elastic and strength parameters reported in this study add to a better understanding of the moisture-dependent mechanical behavior of Chinese fir wood providing valuable material data which can be used for material simulations with consideration of the anisotropic and hygroscopic nature of wood.

The results confirm the general influence of the MC and show that the elastic and strength parameters decrease with increasing MC in all orthotropic directions. However, the impact of moisture on the compliance differs among the individual components. Compared to the Young’s and shear moduli, the Poisson’s ratios do not follow a uniform trend with MC. Using the visualization method for the compliance parameters and yield surface, a clear moisture and orthotropic dependency on compression and tension ability can be displayed. Furthermore, by determining all independent elastic components, not only differences in their moisture sensitivity but also the usually implied symmetry in the non-diagonal elements of the compliance matrix can be found to be an approximation. Therefore, a usable set of anisotropic properties

**Fig. 8** Moisture-dependent yield surfaces of Chinese fir wood in compression (a) and tension (b). Due to the lack of ultimate tensile stress values in  $L$  direction, only yield surfaces at 12.2% MC are shown in  $LR$  and  $LT$  planes in (b)



for macroscopic moisture-dependent elastic and strength material modelling of Chinese fir wood can be provided.

**Acknowledgements** This research was sponsored by the National Natural Science Foundation of China (No. 31570548). J.J. would like to gratefully acknowledge the financial support from the China Scholarship Council (CSC). Special thanks go to Franco Michel and Thomas Schneider for their help during specimen preparation and their expert assistance in conducting the measurements.

#### Compliance with ethical standards

All authors have approved this version of the article and agreed for its submission in your journal. The manuscript has not been published previously, and not under consideration for publication elsewhere. In addition, the authors declare that they fulfill all the ethical responsibilities required by the Committee on Publication Ethics (COPE).

#### References

- Bao FC, Jiang ZH (1998) Wood properties of main tree species from plantation in China. China Forestry Publishing House, Beijing
- Bodig J, Jayne BA (1982) Mechanics of wood and wood composites. Van Nostrand Reinhold Company Inc., New York
- Clauss S, Pescatore C, Niemz P (2014) Anisotropic elastic properties of common ash (*Fraxinus excelsior* L.). Holzforschung 68:941–949
- Dumail JF, Oloffson K, Salmén L (2000) An analysis of rolling shear of spruce wood by the Iosipescu method. Holzforschung 54:420–426
- Gerhards CC (1982) Effect of moisture content and temperature on the mechanical properties of wood: An analysis of immediate effects. Wood Fiber Sci 14:4–36
- Gonçalves R, Trinca AJ, Cerri DGP (2011) Comparison of elastic constants of wood determined by ultrasonic wave propagation and static compression testing. Wood Fiber Sci 43:64–75
- Hering S, Keunecke D, Niemz P (2012a) Moisture-dependent orthotropic elasticity of beech wood. Wood Sci Technol 46:927–938
- Hering S, Saft S, Resch E, Niemz P, Kaliske M (2012b) Characterisation of moisture-dependent plasticity of beech wood and its application to a multi-surface plasticity model. Holzforschung 66:373–380
- Jeong GY, Hindman DP, Zink-Sharp A (2010) Orthotropic properties of loblolly Pine (*Pinus taeda*) strands. J Mater Sci 45:5820–5830
- Keunecke D, Sonderegger W, Pereteanu K, Lüthi T, Niemz P (2007) Determination of Young's and shear moduli of common yew and Norway spruce by means of ultrasonic waves. Wood Sci Technol 41:309–327
- Keunecke D, Hering S, Niemz P (2008) Three-dimensional elastic behavior of common yew and Norway spruce. Wood Sci Technol 42:633–647

- Kretschmann DE, Green DW (1996) Modelling moisture content-mechanical property relationships for clear southern pine. *Wood Fiber Sci* 28:320–337
- McBurney RS, Drow JT (1962) The elastic properties of wood: Young's moduli and Poisson's ratios of Douglas-fir and their relations to moisture content. Forest Product Laboratory, Report No. 1528-D, United States Department of Agriculture, Forest Service, Forest Products Laboratory Madison, Wisconsin
- Mizutani M, Ando K (2015) Influence of a wide range of moisture contents on the Poisson's ratio of wood. *J Wood Sci* 61:81–85
- Neuhaus H (1983) Elastic behavior of spruce wood as a function of moisture content. *Holz Roh-Werkst* 41:21–25
- Niemz P, Caduff D (2008) Research into determination of the Poisson ratio of spruce wood. *Holz Roh-Werkst* 66:1–4
- Östman BAL (1985) Wood tensile strength at temperatures and moisture contents simulating fire conditions. *Wood Sci Technol* 19:103–116
- Ozyhar T, Hering S, Niemz P (2012) Moisture-dependent elastic and strength anisotropy of European beech wood in tension. *J Mater Sci* 47:6141–6150
- Ozyhar T, Hering S, Niemz P (2013a) Moisture-dependent orthotropic tension-compression asymmetry of wood. *Holzforschung* 67:395–404
- Ozyhar T, Hering S, Sanabria SJ, Niemz P (2013b) Determining moisture-dependent elastic characteristics of beech wood by means of ultrasonic waves. *Wood Sci Technol* 47:329–341
- Ozyhar T, Hering S, Niemz P (2013c) Viscoelastic characterization of wood: Time dependence of the orthotropic compliance in tension and compression. *J Rheol* 57:699–717
- Resch E, Kaliske M (2010) Three-dimensional numerical analyses of load-bearing behavior and failure of multiple double-shear dowel-type connections in timber engineering. *Comput Struct* 88:165–177
- Saft S, Kaliske M (2011) Numerical simulation of the ductile failure of mechanically and moisture loaded wooden structures. *Comput Struct* 89:2460–2470
- Tiemann HD (1906) Effect of moisture upon the strength and stiffness of wood. Bulletin of United States Forest Service. United States Government Printing Office, Washington